THE JOURNAL OF PHYSICAL CHEMISTRY B

Article

pubs.acs.org/JPCB

Internal Conversion and Vibrational Energy Redistribution in Chlorophyll A

Prathamesh M. Shenai,[†] Sebastian Fernandez-Alberti,[*,‡] William P. Bricker,[∥] Sergei Tretiak,[§] and Yang Zhao[*,†]

[†]Division of Materials Science, Nanyang Technological University, Singapore, Singapore 639798

[‡]Universidad Nacional de Quilmes, Roque Saenz Pea 352, B1876BXD Bernal, Argentina

[∥]Department of Energy, Environmental and Chemical Engineering, Washington University, Saint Louis, Missouri 63130, United States

[§]Theoretical Division, Center for Nonlinear Studies (CNLS), and Center for Integrated Nanotechnologies (CINT), Los Alamos National Laboratory, Los Alamos, New Mexico 87545, United States

Supporting Information

ABSTRACT: We have computationally investigated the role of intramolecular vibrational modes in determining nonradiative relaxation pathways of photoexcited electronic states in isolated chlorophyll A (ChlA) molecules. To simulate the excited state relaxation from the initially excited *Soret* state to the lowest excited state Q_y, the approach of nonadiabatic excited state molecular dynamics has been adopted. The intramolecular vibrational energy relaxation and redistribution that accompany the electronic internal conversion process is followed by analyzing the excited state trajectories in terms of the ground state equilibrium normal modes. The time dependence of the normal mode velocities is determined by projecting instantaneous Cartesian velocities onto the normal mode vectors. Our analysis of the time evolution of the average mode energies uncovers that only a small subset of the medium-to-high frequency normal modes actively participate in the electronic relaxation processes. These active modes are characterized by the highest overlap with the nonadiabatic coupling vectors (NACRs) during the electronic transitions. Further statistical analysis of the nonadiabatic transitions reveals that the electronic and vibrational energy relaxation occurs via two distinct pathways with significantly different time scales on which the hopping from *Soret* to Q_x occurs thereby dictating the overall dynamics. Furthermore, the NACRs corresponding to each of the transitions have been consistently found to be predominantly similar to a set of normal modes that vary depending upon the transition and the identified categories. Each pathway exhibits a differential time scale of energy transfer and also a differential set of predominant active modes. Our present analysis can be considered as a general approach allowing identification of a reduced subset of specific vibrational coordinates associated with nonradiative relaxation pathways. Therefore, it represents an adequate prior strategy that can particularly facilitates mixed quantum-classical approaches.

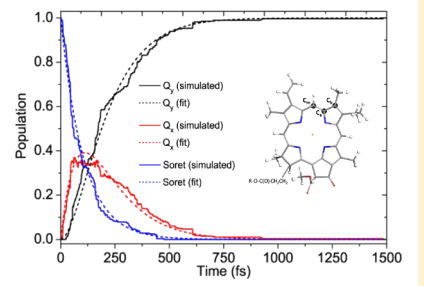

1. INTRODUCTION

Given the supreme importance of natural photosynthesis in sustaining life on the Earth, unraveling its secrets has been a pivotal research area over many decades, especially in the light of depleting conventional energy sources. A sophisticated biological machinery enables harvesting of solar energy and its subsequent conversion to chemical energy inside the thylakoid membranes in the chloroplasts of green plants. Despite the great complexity of the whole process, it is surprisingly hinged upon very few pigment molecules known as chlorophylls. Chlorophylls not only act as primary photoactive pigments and enable energy transfer pathways to the so-called "reaction center" but also participate in charge separation that triggers photochemical conversion.[1,6,7] Dynamics of the photoexcited states in chlorophylls is thus central to a number of aspects of photosynthesis.[8,9]

Previously,[10] we have measured the time constants for high excited states to relax nonradiatively to the lowest excited state (Q_y) in Chlorophyll A (ChlA) and B (ChlB) with ultrafast transient absorption spectroscopy and modeled it using the nonadiabatic excited state molecular dynamics (NA-ESMD) methodology.[64] The slight difference in the molecular structures of these two chlorophylls was found to lead to slightly slower dynamics of $B \rightarrow Q_y$ internal conversion in ChlB in agreement with experimental spectroscopic data.[10] Shi et al. demonstrated that the time-constant for internal conversion increases with an increase in the solvent dielectric constant.[11] Dong et al. further estimated the vibrational relaxation time to be 1.5 ps for ChlA solvated in common solvents such as ethyl

Received: September 30, 2015
Revised: December 8, 2015
Published: December 11, 2015

DOI: 10.1021/acs.jpcb.5b09548
J. Phys. Chem. B 2016, 120, 49−58

acetate and ethyl ether.[12,13] Even though the internal conversion in chlorophylls itself is surprisingly understudied, it has received significant attention in various other light-harvesting pigments such as bacteriochlorophylls,[14−17] carotenoids,[18−22] and porphyrins. Within a wider view, importance of understanding internal conversion is evident from a number of related studies in biological macromolecules such as nucleic acids[23,24] and many other organic/inorganic molecules or compounds.[25,30,31]

Nonradiative relaxation of excited electronic states is invariably accompanied by vibrational energy redistribution, and a number of studies point to the importance of "active" vibrational modes in assisting internal conversion processes.[32−36] Experimentally, such studies are generally based on variants of excited state IR spectroscopy,[37−39] ultrafast time-resolved IR spectroscopy,[40−42] and ultrafast transient IR spectroscopy.[43] These techniques have been shown to be powerful in the study of the excited states decay.[47−57] Much of the theoretical work on intramolecular energy transfer in organic molecules has involved classical and semiclassical Hamiltonians using harmonic approximations to identify the pathways and life times of energy transfer out of a given bond or mode.[44−46] Equilibrium normal modes (ENMs), typically calculated from second derivatives of the ground-state (GS) energy with respect to nuclear coordinates (Hessian), can be used to elucidate vibrational motions of polyatomic molecules.[58−61] Within this theoretical framework, one can then address the vibrational energy flow by following the time evolution of the kinetic energy of each ENM. Anharmonic effects and mode couplings have, however, been recognized to be important toward giving rise to vibrational energy redistribution. Previous work has extensively discussed these aspects in proteins.[26−29] In particular, for ChlA, for example, density functional theory calculations have been used to investigate the vibrational properties and to ascertain couplings between important infrared-active modes of the carbonyl groups.[3,62] In this work, following up on our earlier study, we focus on characterizing the role of vibrational energy redistribution in the nonradiative relaxation of high-energy excited states in ChlA. Our aim is to identify the nature of active normal modes related to the electronic couplings and intramolecular energy transfer throughout the nonadiabatic excited-state molecular dynamics. We show that only a small subset of vibrational modes of ChlA actively aid the internal conversion process.

The remainder of the paper is organized as follows. The underlying theory for the NA-ESMD methodology is briefly described in the next section 2. Results are presented and discussed in detail in section 3 before drawing concluding remarks in the final section, section 4.

2. THEORETICAL AND COMPUTATIONAL DETAILS

2.1. NA-ESMD Background. The NA-ESMD framework[63,64] allows for simulation of photoinduced dynamics of large organic conjugated molecules involving multiple coupled electronic excited states, a formidable task carried out by combining the molecular dynamics with quantum transitions approach[65,66] with "on the fly" analytical calculations of excited-state energies,[67−69] gradients,[70,71] and nonadiabatic coupling[63,72−74] terms. For this purpose, the collective electron oscillator (CEO) method[75−78] is applied using the AM1 semiempirical Hamiltonian[79,80] at the configuration interaction singles level.[81,82] Previously, AM1 and similar semiempirical models have been successfully applied to describe excited state properties of porphyrin-based molecules.[80,83−91] A detailed discussion on the implementation of, the advantages of, and various testing parameters of NA-ESMD can be found elsewhere.[63,64,97]

2.2. Normal Mode Analysis. ENMs are computed at the ground state state minimum $\mathbf{R}_0$ from the mass-weighted Hessian matrix $\mathbf{H}$ with elements

$$\mathbf{H}_{ij}(\mathbf{R}_0) = -\partial^2 E/\partial q_i \partial q_j \tag{1}$$

where E is the ground state potential energy and $q_i = \sqrt{m_i}(R_i - R_{0,i})$ is the mass weighted Cartesian displacement of ith atom with mass m_i and Cartesian coordinates $R_{0,i}(X_{0,i}, Y_{0,i}, Z_{0,i})$.[92−,94,96,98−102] Geometry optimization was performed on the chlorophyll molecule with the phytyl tail replaced by a methyl group for computational ease, with the AM1 semiempirical Hamiltonian, using Gaussian 09.[103] Diagonalization of $\mathbf{H}$ produces the set of orthonormal ENM with frequencies ν_i related to the eigenvalues $\lambda_i (i = 1, ..., 3N - 6)$ of $\mathbf{H}$ as $\nu_i = (\sqrt{\lambda_i}/2\pi)$. ENMs are defined in a body-fixed reference frame with the origin at the center of mass of the molecule and axes corresponding to its principle axes of inertia. Upon diagonalization of $\mathbf{H}$, the set of ENM vectors $\{Q_i\}$, $i = 1$, $3N - 6$ are obtained from the corresponding eigenvector matrix $\mathbf{L}$, which allows to express their amplitudes throughout the NA-ESMD as a linear combination of the set $\{q_i\}_{i=1,3N}$ as

$$Q_i(t) = \sum_{j=1}^{3N} l_{ji} q_j(t) \qquad i = 1, \ ..., \ 3N - 6 \tag{2}$$

where l_{ji} are elements of the eigenvector matrix $\mathbf{L}$. By differentiating this expression with respect to time, we obtain the relationship between the momenta

$$\dot{Q}_i(t) = \sum_{j=1}^{3N} l_{ji} \dot{q}_j(t) \qquad i = 1, \ ..., \ 3N - 6 \tag{3}$$

In this way, the vibrational kinetic energy transforms in terms of the ENM momenta as

$$K(t) = \frac{1}{2} \sum_{i=1}^{3N-6} (\dot{Q}_i(t))^2 \tag{4}$$

The total vibrational energy associated with a given mode is calculated using the virial theorem, $E_i(t) = 2K_i(t)$.

2.3. Molecular Dynamics Simulations. The ground state molecular dynamics simulation was then performed at 300 K with a time step $\Delta t = 0.5$ fs. The system was heated to allow thermal equilibration at a final temperature of 300 K during the first 10 ps. The Langevin equation at constant temperature was utilized with a friction coefficient of $\gamma = 2.0$ ps. This value has been chosen to allow an efficient temperature coupling[95] to obtain the adequate ground state conformational sampling. In the 8 ns long production run following equilibration, we sample atomic coordinates and momenta at every 20 ps generating a set of 400 initial positions and momenta for the subsequent NA-ESMD simulations. Details of the assignment of the initial excited state for each NA-ESMD trajectories according to a Franck−Condon window centered at 2.94 eV (lowest state in the Soret band) can be found elsewhere.[10] As opposed to the initial ground state simulation, NA-ESMD simuations have been carried out at constant energy during 1.5 ps using a

DOI: 10.1021/acs.jpcb.5b09548
J. Phys. Chem. B 2016, 120, 49−58

classical time-step of Δt = 0.1 fs and N_q = 4 quantum time steps per classical step to simultaneously propagate the electronic coefficients for the 10 lowest excited states. The existence of trivial unavoided crossings has been examined by tracking the identities of the states.[104]

3. RESULTS AND DISCUSSIONS

We have investigated the dynamics of the internal conversion process of ChlA (Figure 1a) that takes place after its initial photoexcitation in the red edge (S_3) of the *Soret* (B) band (see Figure 1b). Subsequent to laser excitation, the molecular system experiences a fast $B \rightarrow Q_x \rightarrow Q_y$ electronic energy relaxation and redistribution that involves the selective participation of specific atomic groups and complex global migration of the electronic wave function within the total carbon macrocycle of the porphyrin ring structure.[10] Figure 1c represents the average populations of various electronic states as a function of time. Here, the population of the *Soret* state is taken to be a summation of the populations on S_3 and S_4 as a small percentage (<4%) of configurations are initially excited at S_4. The lowest excited state is completely populated within 1.5 ps. By fitting the simulations data with a sequential kinetic model we can extract the time constant as τ_1 = 105 fs for the *Soret* $\rightarrow Q_x$ process and τ_2 = 124 fs for the $Q_x \rightarrow Q_y$ relaxation. The time constants obtained through the constant energy simulations are close to those obtained by us in the previous study using constant temperature simulations.

The intramolecular vibrational energy flow in ChlA, accompanied by the electronic energy transfer, is monitored by evaluating the time evolution of the normal mode velocities obtained by projection of the body-fixed mass weighted Cartesian velocities onto the normal modes vectors (see Section Normal Mode Analysis).

Parts a and b of Figure 2 show the vibrational energy E_i along different intermediate-range and high-frequency ENMs (twice the kinetic energy considering the equipartition of energy) averaged over the ensemble of NA-ESMD trajectories. It is observed first that the intramolecular vibrational energy redistribution is not statistical, since the energy deposited in each ENM varies significantly. It is important to stress that, in the present work, NA-ESMD simulations have been performed at constant energy. Therefore, the lack of dominant vibronic relaxation paths during the internal conversion process should lead to transient and final accumulations of slightly different amounts of the initial excess of energy spread among all the 240 vibrational normal modes of the molecule. Except for the 191th to 201th, and also 180th and 182th ENMs, the energies of all other ENMs deviate only slightly from their equilibrium values during the internal conversion process. We have defined a normal mode as active during the internal conversion process if, at any time during the NA-ESMD simulations, its average energy exceeds twice the initial kT = 0.026 eV equilibrium value, thus reflecting a strong coupling to the electronic degrees

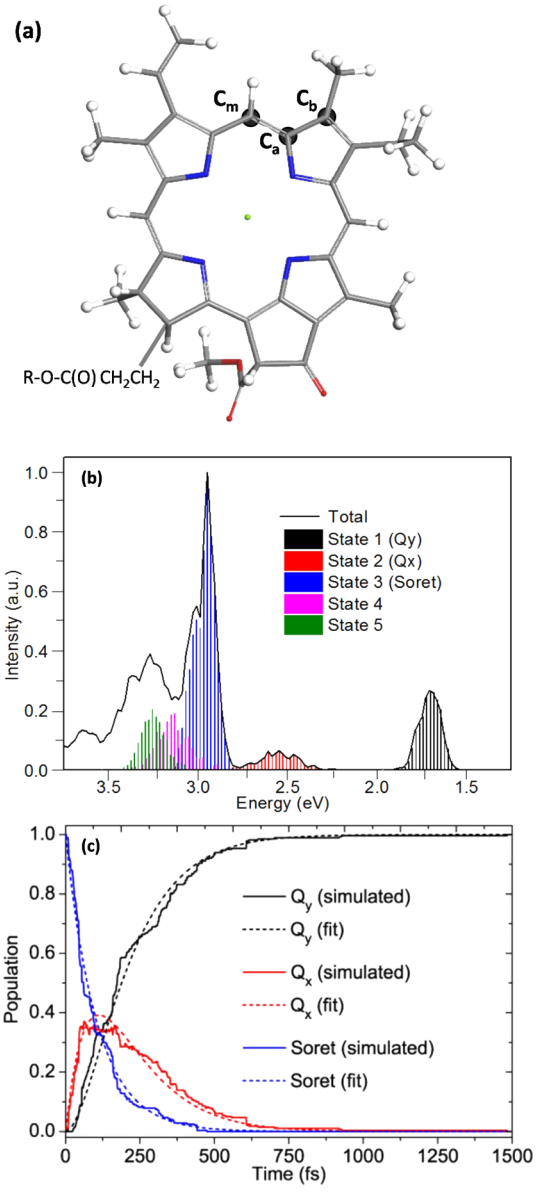

Figure 1. (a) Molecular structure of chlorophyll A (carbon atoms in gray, oxygen in red, nitrogen in blue, magnesium in green and hydrogen in light gray), where R denotes the phytyl tail. (b) Simulated absorption spectrum of ChlA where contributions from the 5 lowest energy exited states have been included; and (c) Populations of excited states following initial excitation centered at the lowest state in the *Soret* band. Results are fitted (dashed curves) with a sequential kinetic rate constant model.

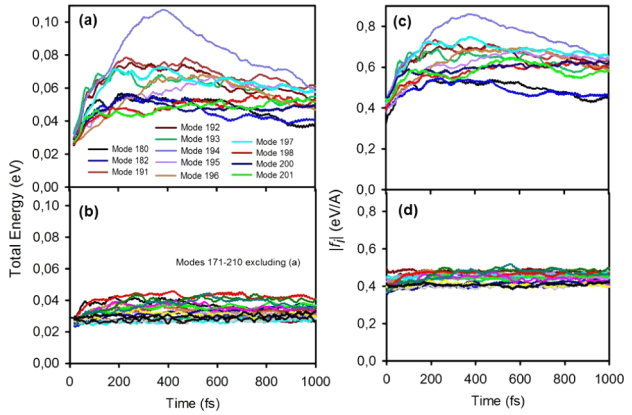

Figure 2. Time evolution of the total energy of trajectories along (a) normal modes 180, 182, and 191−201 and (b) all the normal modes from 171 to 210 excluding those plotted in part a; time evolution of the norm of the normal mode forces averaged over the trajectories for (c) normal modes 180, 182, 191−201; (d) all the normal modes from 171 to 210 excluding those plotted in part c.

DOI: 10.1021/acs.jpcb.5b09548
J. Phys. Chem. B 2016, 120, 49−58

of freedom. These reduced number of active modes experience a fast increase in their energy reaching their maxima at about 400 fs. The maximum combined energy stored in all of these active modes is 0.874 eV (7049 cm^{-1}, with the highest contribution coming from mode 194 at 0.108 eV (871 cm^{-1}). After that, they experience a slow energy relaxation that is extended for more than 1 ps. The rest of the modes seems to act as a bath of coupled harmonic oscillators to which the excess of energy, transiently accumulated in these active modes, is finally transferred.

A careful analysis along each of the 240 normal modes reveals that only a small subset of them indexed predominantly from modes number 180 (1465 cm^{-1}), 182 (1491 cm^{-1}), and 191−201 (1665−1908 cm^{-1}) are strongly excited during the excited state relaxation process as shown in Figure 2a. The energy plots in Figure 2b along any of the remaining normal modes in a similar frequency bracket suggest that they are not involved in the excited state dynamics. We have thus identified a few vibrational modes that are intricately associated with *Soret* to Q_y internal conversion in ChlA. These modes can be associated with the 1597−1620 cm^{-1} band observed in the IR spectra of most chlorophyll systems.[2,3] This assignment is based on previous work performed by Wang and co-workers.[3] Despite the frequency difference between the experimental IR band and the calculated one, the assignment can be performed based on the common relative nuclear displacements between vibrations associated with this experimental band and relative nuclear displacements involved in the active normal modes. On the basis of the normal mode assignments performed by Boldtet al.,[5] this band is predominantly associated with C_aC_m, C_aC_b, and C_bC_b stretching vibrations (see Figure 1a).[4,5]

Parts c and d of Figure 2 show the time-dependence of the norm of different ENM forces averaged over the trajectories. Thereof we can point out the role that gradients/forces on the excited states play during this intramolecular vibrational energy redistribution. Upon vertical excitation to the Soret band, an ultrafast transfer of electronic to vibrational energy is observed as an increase of the forces in the direction of the modes previously identified as active normal modes. The relative low initial values of these forces increase in time until they reach their maxima at about 400 fs. This behavior indicates that the redistribution of the energy does not take place as the result of the initial ultrafast adiabatic relaxation that occurs right after photoexcitation, but rather as a consequence of nonadiabatic dynamics.

In order to further elucidate the role played by these vibrational normal modes in the internal conversion process, we investigate the correspondence between such active modes and the nonadiabatic coupling vectors (NACRs) defined as

$$d_{IJ} = \langle \psi_I(r, R) | \nabla_R \psi_J(r, R) \rangle \quad (5)$$

where r and R are the electronic and nuclear vector coordinates, respectively, and $\psi_I(r, R)$ is the Ith CI electronic state.

The direction of NACR can be interpreted as the nonadiabatic contribution to the direction of the main driving force on the nuclei during electronic transitions.[33] Figure 3 depict the projection of the forces on the direction of NACR throughout the NAESMD simulations. After photoexcitation, the molecular system enters in regions of the configurational phase space with strong nonadiabatic couplings. The nonadiabatic contributions to the nuclear forces rapidly increase in time. At earlier times, the direction of NACR(Soret-Q_x)

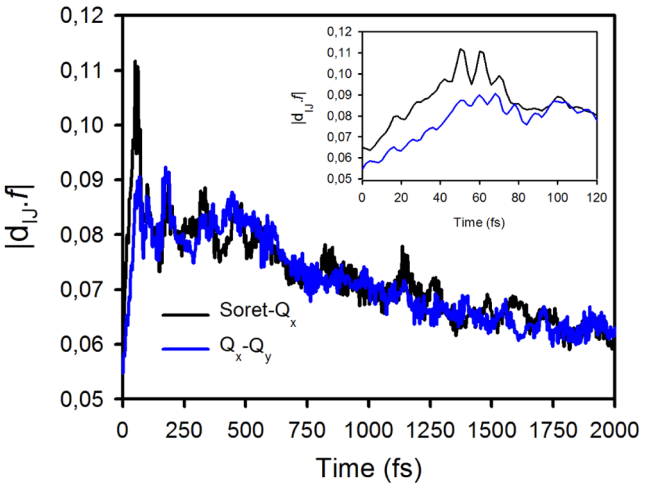

Figure 3. Time evolution of the projection of the forces on the direction of NACR averaged over the trajectories.

represents a higher contribution than the NACR(Q_x−Q_y) one. After the first 100 fs of the simulations, the nonadiabatic contributions of either NACR(Soret-Q_x) and NACR(Q_x−Q_y) persist at relatively higher values during the next 400 fs. After that, both contributions decay while the system adiabatically relaxes on the Q_y state. Therefore, the nonadiabatic contribution of the nuclear forces seems to dictate the fast intramolecular vibrational energy redistribution that occurs during the internal conversion process. During nonadiabatic dynamics in the vicinity of level crossings, both the Pechukas forces and redistribution of electronic energy excess upon quantum transitions are generally raising classical momenta of nuclei in the direction of NACR vectors. This ensures an effective flow of electronic energy into specific vibrational modes aligned with NACR vectors.

It is interesting at this point to associate each step of the *Soret* to Q_y internal conversion with the participation of the different active normal modes in the corresponding concomitant intramolecular vibrational energy pathways. To this end, from the ensemble of excited state trajectories, we first analyze two sets of NACRs - one corresponding to the *Soret* to Q_x transition and the other corresponding to the Q_x to Q_y relaxation. Each NACR vector, expressed in body-fixed reference frame, is projected on the basis of normal modes $\{Q_i\}_{i=1,3N-6}$. In Figure 4, we show the distributions of the overlap between NACR vectors and various selected normal modes. Figure 4a indicates a considerable overlap (>20%) between a substantial subset of *Soret* to Q_x NACRs and only a few normal modes indexed 192 and 194 while the overlap with the other modes is relatively small. On the other hand, for Q_x to Q_y transition, the overlaps between the NACRs and only the normal modes 180, 191, 192, and 193 are significant as shown in Figure 4b. This implies that the nuclear motions that modulate the electronic couplings, and therefore contribute to the ultrafast electronic energy transfer, involve directions given by only a few normal modes of intermediate-to-high frequencies. Besides, these modes that overlap the most with the NACR vectors, are in agreement with our previously identified active modes due to the significant accumulation of the excess vibrational energy during the relaxation process.

It is worth to mention that, according to the surface hopping prescription,[65,105,106] adjustments to the nuclear velocities are required in order to conserve total energy following hops

DOI: 10.1021/acs.jpcb.5b09548
J. Phys. Chem. B 2016, 120, 49−58

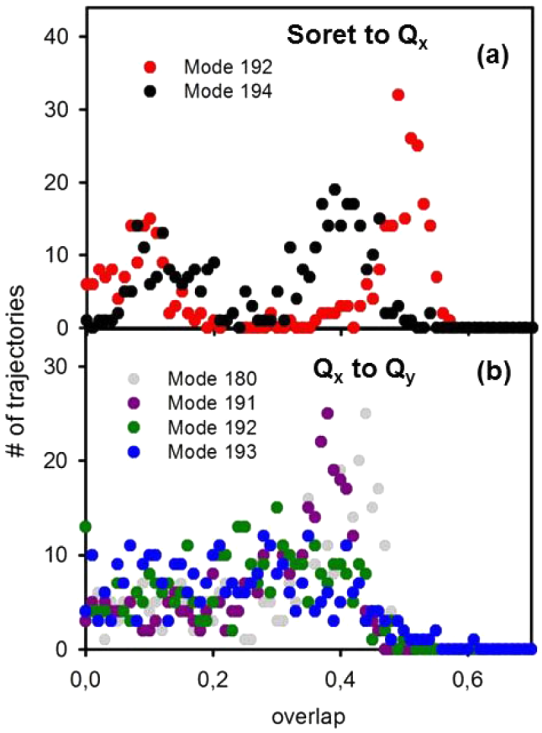

Figure 4. Distribution of the values of overlaps between specific normal modes and the set of NACRs corresponding to (a) *Soret* to Q_x and (b) Q_x to Q_y transitions.

between electronic states. The direction in which the velocity $\dot{R}_i$ of each of the ith atom in the molecular system is commonly rescaled, corresponds to the direction of the NACR vector. Via an important test of reliability, we have ensured that changing the rescaling prescription does not alter the results of the dynamics (see Supporting Information).

For a more quantitative characterization of the electronic and vibrational energy pathways, representative NACR vectors associated with each $I \rightarrow J$ transition can be defined. We construct matrices $\mathbf{A}_{IJ}$ of dimension $3N \times K$, with K being the number of trajectories with an effective $I \rightarrow J$ hop. Matrices $\mathbf{A}_{IJ}$ are built with columns representing the NACR vector at the moment of effective $I \rightarrow J$ transition in each of the K NA-ESMD trajectories. As these are not square matrices, in order to capture the representative NACR vectors of the whole set, Singular Value Decomposition (SVD) of $\mathbf{A}_{IJ}$ can be performed. Essentially it means that $\mathbf{A}_{IJ}$ is written as the product of a $3N \times K$ column-orthogonal matrix $\mathbf{U}$, a $K \times K$ diagonal matrix $\mathbf{W}$ with positive or zero elements (the singular values), and the transpose of a $K \times K$ orthogonal matrix $\mathbf{V}$:

$$[A_{IJ}] = [U_{IJ}] \cdot [W_{IJ}] \cdot [V_{IJ}^{T}] \tag{6}$$

Thus, the a_{IJ}^{ij} elements of the matrix $\mathbf{A}_{IJ}$ can be expressed as the sum of products of columns of $\mathbf{U}_{IJ}$ and rows of $\mathbf{V}_{IJ}^{T}$, with the "weighting factors" being the singular values w_l^{IJ}

$$a_{IJ}^{ij} = \sum_{l=1}^{k} w_l^{IJ} \cdot u_{IJ}^{il} \cdot N_{IJ}^{jl} \tag{7}$$

Subsequently, in this work, the u_{IJ}^{l} vectors, in the decreasing order of the values of w_l^{IJ}, are referred to as lth SVD vectors. The eigenvalues w_l^{IJ} indicate the correspondence between the entire data set and the individual SVD vectors. Here we find that the first two SVD vectors, shown in Figure 5, with the largest eigenvalues can sufficiently well describe more than 80%

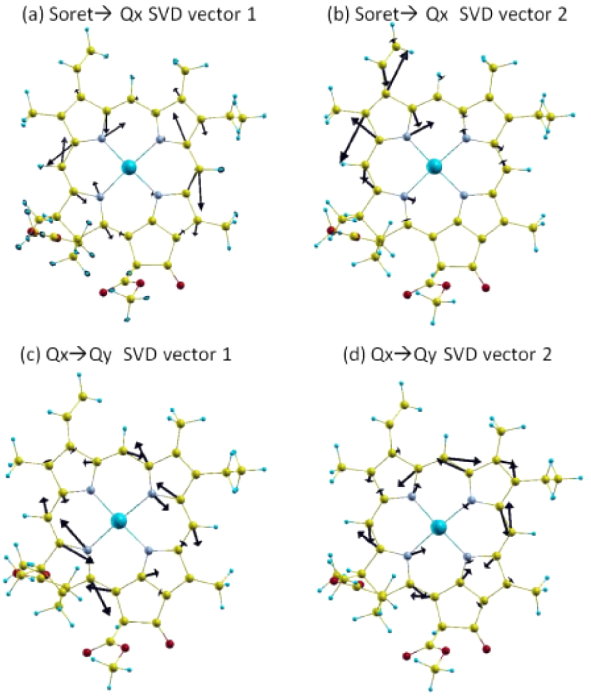

Figure 5. Visualization of the first two SVD vectors for the NACRs corresponding to (a, b) *Soret* to Q_x and (c, d) to Q_x to Q_y internal conversion.

of the NACRs from the ensemble. An intuitive understanding of the SVD vectors can be obtained by plotting the overlap between an NACR and the first SVD vector 1 (SVD1) versus the overlap between the same NACR and SVD2. Figure 6

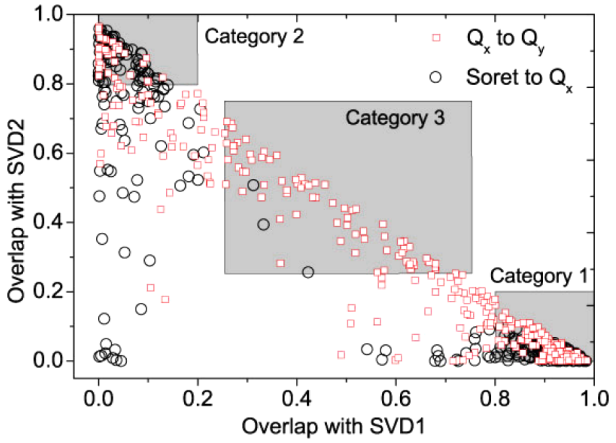

Figure 6. Overlap of each of the NACRs from the ensemble with the first SVD vector versus the overlap with the second SVD vector for *Soret* to Q_x (circles) and for Q_x to Q_y (squares) transitions.

shows that for the *Soret* to Q_x transition the complete set of NACRs can be distinctly categorized in two subsets—one (containing nearly 70% of the total NA-ESMD trajectories) which shows close resemblance with the SVD1 and the other with a very high overlap with the SVD2. This indicates that the *Soret* to Q_x transition may take place along two different pathways characterized by two different NACRs and sub-

DOI: 10.1021/acs.jpcb.5b09548
J. Phys. Chem. B 2016, 120, 49−58

sequently, the excited state dynamics along the two paths may exhibit important differences. Therefore, SVD1 and SVD2 vectors can be considered as an average representation of two distinguished original ensembles of NACR vectors, each of them identified with a particular *Soret* to Q_x transition. On the other hand, for the Q_x to Q_y transition, while the whole data set can still be represented by the first two SVD vectors, a distinct categorization does not emerge. The NACRs for this process are uniform combinations of SVD1 and SVD2. The subspace (plane) formed by both SVD vectors contains the overall ensemble of NACR vectors associated with the *Soret* to Q_x transition. According to the structural diagram of Chla that can be found elsewhere,[4] these vectors contain substantial contributions from C_aC_m, C_aC_b, and C_bC_b stretching vibrations[4,5] that are associated with the IR spectra band observed at 1597−1620 cm^{-1}.[2,4]

In order to ascertain whether the two distinct NACRs lead to two different relaxation pathways, we segregated the excited state dynamics trajectories based on the following criterion. Category 1 contains trajectories for which the NACRs exhibit more than 80% overlap with SVD1 for a given transition whereas Category 2 contains trajectories for which the NACRs show greater than 80% overlaps with SVD2. A third category relevant only to the Q_x to Q_y transition accounts for those trajectories for which the NACRs are a mixture of the first two SVD vectors. The shaded regions in Figure 6 also provide a visual aid to this categorizations. Figures 7a,b show the

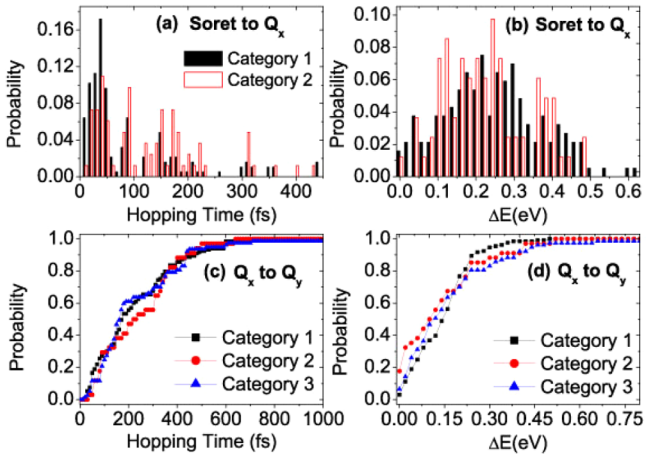

Figure 7. Probability distribution of the (a) hopping times and (b) ΔE at the time of hopping during *Soret* to Q_x transition for different categories based on SVD analysis described in text. For Q_x to Q_y transition, the corresponding plots for (c) hopping times and (d) ΔE as cumulative distributions.

probability distribution of the hopping time and the difference in the energies at the time of hopping (ΔE), respectively, for the two categories of the *Soret* to Q_x internal conversion. The distribution of ΔE can be seen to be relatively similar for both the categories, with the average value equal to 0.2554 eV for category 1 and 0.2343 eV for category 2. In order to clarify whether degeneracy (with $\Delta E = 0$) can be reached by any of these two pathways, we adopt an arbitrary limit of $\Delta E < 0.1$ eV to separate cases of strict degeneracy or their immediate regions and cases with larger ΔE. With this separation in mind, we can say that less than only 16% of trajectories corresponding to each relaxation pathway pass through the degeneracy. The distributions of the hopping times are, however, significantly different. This distinction becomes readily apparent in the average hopping time, which is much greater for category 2 trajectories (131.87 fs) than that for category 2 (90.93 fs). Both of these properties are however much more homogeneous for the Q_x to Q_y relaxation across all 3 categories as evident in the cumulative probability plots in Figure 7c,d. We have also subjected all of these distributions to the Kolmogorov−Smirnov test, which allows for an objective assessment of the similarity between any two distributions and have found that it shows that only the distributions in Figure 7a are distinct. We thus find that the *Soret* to Q_x transition occurs along two different pathways characterized by distinct NACRs. However, once the system reaches state Q_x, the subsequent relaxation process has uniform characteristics. Furthermore, we have calculated the population evolution on the different trajectory subsets based on the two categories obtained via SVD analysis of only the *Soret* to Q_x transition. The resulting plots shown in Figure 8 clearly point to the entirely different time scales of

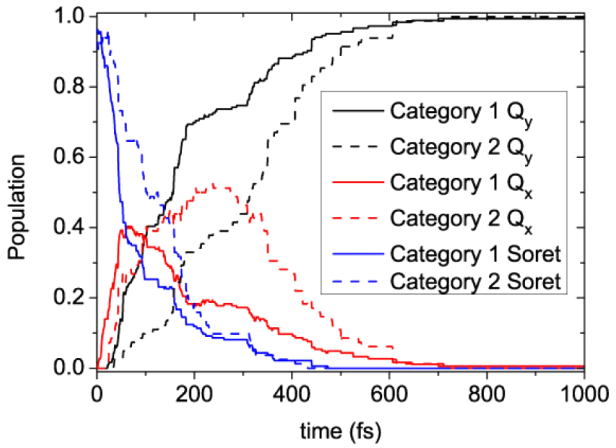

Figure 8. Excited state dynamics for *Soret* to Q_x internal conversion for category 1 trajectories (solid curves) and category 2 trajectories (dashed curves).

both *Soret* to Q_x and the Q_x to Q_y internal conversion processes in the two categories. The time constant extracted via fitting simulated data with a sequential kinetic model is found to be 89.0 fs for category 1 trajectories and 133.3 fs for category 2 trajectories for the *Soret* to Q_x transition. For the Q_x to Q_y transition, the time constants are 94.4 and 187.3 fs for category 1 and 2, respectively.

Finally, we analyze the relationship between the categorization of the NA-ESMD trajectories for the two-stepped internal conversion process and the subset of the active normal modes identified earlier. We thus calculate the overlaps between the selected normal modes and the NACRs corresponding to each of the two transitions and average them within different ensembles determined by the aforementioned SVD based categorization. Table 1 lists the obtained results for all those active modes which appear in more than 90% of the trajectories within each category. For easier comparison, the most important modes, which show an overlap close to or higher than 0.25, are highlighted in bold. For the *Soret* to Q_x transition we can observe that the active modes are distinctly different for the two categories. Considering that the categorization is based on the SVD vectors, this implies that the *Soret* to Q_x transition is associated with two distinct NACRs that resemble different sets of normal modes. Furthermore, as

DOI: 10.1021/acs.jpcb.5b09548
J. Phys. Chem. B 2016, 120, 49−58

Table 1. Average Values of Overlaps between Various Normal Modes and the NACRs Corresponding to *Soret* to Q_x and Q_x to Q_y Transitions[a]

	Soret to Q_x		Q_x to Q_y		
mode	cat 1	cat 2	cat 1	cat 2	cat 3
180	**0.269**	–	**0.436**	–	**0.289**
188	–	**0.317**	0.118	–	–
189	0.175	–	**0.299**	–	0.210
191	**0.300**	0.215	**0.391**	–	**0.272**
192	**0.502**	–	**0.334**	0.204	**0.253**
193	–	**0.238**	–	**0.335**	**0.301**
194	**0.403**	–	–	**0.284**	0.213
195	–	**0.281**	**0.243**	–	–
198	–	–	0.172	0.162	–
199	0.147	–	0.172	**0.251**	–
200	0.188	**0.272**	–	**0.424**	**0.276**
201	0.142	**0.428**	–	**0.311**	**0.241**

[a]Overlap values are shown for only those active modes which appear in >90% of the trajectories under each category. The values in bold emphasize the most important modes showing an overlap nearly equal to or greater than 0.25.

Figure 4a shows, the normal modes with prominent overlaps with the *Soret* to Q_x NACRs are indexed 192 and 194, which is consistent with the fact that nearly 70% of the trajectories belong to category 1. Modes 191, 192, and 194 are indeed also those, along which the strongest modulations of total energies are observed in Figure 2a. For the Q_x to Q_y transition as well one can note the distinctness of participating normal modes between category 1 and 2. However, the presence of the third category lends a significantly more mixed character that is consistent with the results presented in Figure 4b.

4. CONCLUSIONS

We have identified the normal modes that participate actively in the intramolecular electronic energy relaxation and redistribution during the internal conversion process of the pigment chlorophyll A after its photoexcitation to the Soret band. The intramolecular vibrational energy flow, concomitant with the electronic energy transfer, is monitored by evaluating the temporal variance of the energy in each individual normal mode. Our analysis indicates that this process is not statistical, since the energy deposited on each mode varies significantly. Only a small subset of intermediate-to-high-frequency normal modes, with the highest overlap with the nonadiabatic coupling vectors at the instant of effective hops, experience a substantial increase in their vibrational energy during the process. Therefore, velocity adjustments, performed according to the surface hopping prescription, in the direction of the nonadiabatic coupling vectors can be well validated by the confirmation that this direction is the main vibrationally active direction during the internal conversion process. Two distinct pathways for nonradiative relaxation have been discovered, involving two different sets of active normal modes and significantly different time scales for the $S_3 \rightarrow S_2$ transition. We consider that this present analysis can be used as a general approach allowing identification of a reduced subset of specific vibrational coordinates associated with nonradiative relaxation pathways. It is our hope that results reported here shall inspire further developments of hybrid quantum-classical molecular dynamics simulations in extended conjugated molecules that deal explicitly with the quantum mechanical treatment of a small subset of normal modes and the conventional classical treatment of the remaining degrees of freedom.

■ ASSOCIATED CONTENT

Supporting Information

The Supporting Information is available free of charge on the ACS Publications website at DOI: 10.1021/acs.jpcb.5b09548.

Description of a modified method for the rescaling of nuclear velocities as well as the results from a set of simulations with the modified algorithm (PDF)

■ AUTHOR INFORMATION

Corresponding Authors

*(S.F.-A.) E-mail: sfalberti@gmail.com.

*(Y.Z.) Telephone: +(65) 65137990. E-mail: yzhao@ntu.edu.sg.

Notes

The authors declare no competing financial interest.

■ ACKNOWLEDGMENTS

P.M.S and Y.Z. acknowledge support from Singapore National Research Foundation through the Competitive Research Programme (CRP) under Project No. NRF-CRP5-2009-04. S.F.-A is supported by CONICET, UNQ, ANPCyT (PICT-2014-2662). S.T. acknowledges support from Los Alamos National Laboratory (LANL) Directed Research and Development Funds. Los Alamos National Laboratory is operated by Los Alamos National Security, LLC, for the National Nuclear Security Administration of the U.S. Department of Energy under Contract DEAC52-06NA25396. We acknowledge support of the Center for Integrated Nanotechnology (CINT), an Office of Basic Energy Sciences, U.S. Department of Energy, user facility.

■ REFERENCES

(1) Blankenship, R. E. *Molecular Mechanisms of Photosynthesis*; Blackwell Publishing: Williston, VT, 2002.

(2) Katz, J. J.; Dougherty, L.; Boucher, L. In *The Chlorophylls*; Vernon, L. P., Seely, G. R., Eds.; Academic Press: New York, 1966; pp 185–251.

(3) Wang, R.; Parameswaran, S.; Hastings, G. Density functional theory based calculations of the vibrational properties of chlorophyll-a. *Vib. Spectrosc.* **2007**, *44*, 357–368.

(4) Thomas, L. L.; Kim, J. H.; Cotton, T. M. Comparative study of resonance ramman and surface-enhanced resonance raman Chlorophyll a spectra using Soret and red excitation. *J. Am. Chem. Soc.* **1990**, *112*, 9378–9386.

(5) Boldt, N. J.; Donohoe, R. J.; Birge, R. R.; Bocian, D. F. Chlorophyll model compounds: Effects of ow symmetry on the Resonance Raman spectra and normal mode descriptions of Nickel(II) dihydroporphyrins. *J. Am. Chem. Soc.* **1987**, *109*, 2284–2298.

(6) Croce, R.; van Amerongen, H. Natural strategies for photosynthetic light harvesting. *Nat. Chem. Biol.* **2014**, *10*, 492–501.

(7) Scholes, G. D.; Fleming, G. R.; Olaya-Castro, A.; van Grondelle, R. Lessons from nature about solar light harvesting. *Nat. Chem.* **2011**, *3*, 763–774.

(8) Niyogi, K. K. Photoprotection revisited: Genetic and molecular approaches. *Annu. Rev. Plant Physiol. Plant Mol. Biol.* **1999**, *50*, 333–359.

(9) Ruban, A. V.; Johnson, M. P.; Duffy, C. D. P. The photoprotective molecular switch in the photosystem II antenna. *Biochim. Biophys. Acta, Bioenerg.* **2012**, *1817*, 167–181.

(10) Bricker, W. P.; Shenai, P. M.; Ghosh, A.; Liu, Z.; Enriquez, M. G. M.; Lambrev, P. H.; Tan, H. S.; Lo, C. S.; Tretiak, S.; Fernandez-

DOI: 10.1021/acs.jpcb.5b09548
J. Phys. Chem. B 2016, 120, 49–58

Alberti, S.; et al. Non-radiative relaxation of photoexcited chlorophylls: theoretical and experimental study. *Sci. Rep.* **2015**, *5*, 13625.
(11) Shi, Y.; Liu, J. Y.; Han, K. L. Investigation of the internal conversion time of the chlorophyll a from S3, S2 to S1. *Chem. Phys. Lett.* **2005**, *410*, 260−263.
(12) Dong, L. Q.; Niu, K.; Cong, S. L. Theoretical study of vibrational relaxation and internal conversion dynamics of chlorophyll-a in ethyl acetate solvent in femtosecond laser fields. *Chem. Phys. Lett.* **2006**, *432*, 286−290.
(13) Dong, L. Q.; Niu, K.; Cong, S. L. Theoretical analysis of internal conversion pathways and vibrational relaxation process of chlorophyll-a in ethyl ether solvent. *Chem. Phys. Lett.* **2007**, *440*, 150−154.
(14) Kosumi, D.; Maruta, S.; Fujii, R.; Kanemoto, K.; Sugisaki, M.; Hashimoto, H. Ultrafast excited state dynamics of monomeric bacteriochlorophyll a. *Phys. Status Solidi C* **2011**, *8*, 92−95.
(15) Kosumi, D.; Nakagawa, N.; Sakai, S.; Nagaoka, Y.; Maruta, S.; Sugisaki, M.; Dewa, T.; Nango, M.; Hashimoto, H. Ultrafast intramolecular relaxation dynamics of Mg- and Zn-bacteriochlorophyll a. *J. Chem. Phys.* **2013**, *139*, 034311.
(16) Musewald, C.; Hartwich, G.; Lossau, H.; Gilch, P.; Pöllinger-Dammer, F.; Scheer, H.; Michel-Beyerle, M. E. Ultrafast photophysics and photochemistry of [Ni]-bacteriochlorophyll a. *J. Phys. Chem. B* **1999**, *103*, 7055−7060.
(17) Lambrev, P. H.; Miloslavina, Y.; van Stokkum, I. H. M.; Susz, A.; Tworzydlo, J.; Fiedor, J.; Huhn, G.; van Grondelle, R.; Garab, G.; Fiedor, L. Excitation Energy Trapping and Dissipation by Ni-Substituted Bacteriochlorophyll a in Reconstituted LH1 Complexes from Rhodospirillum rubrum. *J. Phys. Chem. B* **2013**, *117*, 11260−11271.
(18) Macpherson, A. N.; Gillbro, T. Solvent dependence of the ultrafast S2-S1 internal conversion rate of beta-carotene. *J. Phys. Chem. A* **1998**, *102*, 5049−5058.
(19) Cerullo, G.; Polli, D.; Lanzani, G.; De Silvestri, S.; Hashimoto, H.; Cogdell, R. J. Photosynthetic light harvesting by carotenoids: Detection of an intermediate excited state. *Science* **2002**, *298*, 2395−2398.
(20) Polli, D.; Cerullo, G.; Lanzani, G.; De Silvestri, S.; Yanagi, K.; Hashimoto, H.; Cogdell, R. J. Conjugation length dependence of internal conversion in carotenoids: Role of the intermediate state. *Phys. Rev. Lett.* **2004**, *93*, 163202.
(21) Kosumi, D.; Komukai, M.; Hashimoto, H.; Yoshizawa, M. Ultrafast dynamics of all-trans-beta-carotene explored by resonant and nonresonant photoexcitations. *Phys. Rev. Lett.* **2005**, *95*, 213601.
(22) Perez Lustres, J. L. P.; Dobryakov, A. L.; Holzwarth, A.; Veiga, M. S2 to S1 internal conversion in beta-carotene: Strong vibronic coupling from amplitude oscillations of transient absorption bands. *Angew. Chem., Int. Ed.* **2007**, *46*, 3758−3761.
(23) Pecourt, J. M. L.; Peon, J.; Kohler, B. DNA excited-state dynamics: Ultrafast internal conversion and vibrational cooling in a series of nucleosides. *J. Am. Chem. Soc.* **2001**, *123*, 10370−10378.
(24) Pecourt, J. M. L.; Peon, J.; Kohler, B. Ultrafast internal conversion of electronically excited RNA and DNA nucleosides in water. *J. Am. Chem. Soc.* **2000**, *122*, 9348−9349.
(25) Fidder, H.; Rini, M.; Nibbering, E. T. J. The role of large conformational changes in efficient ultrafast internal conversion: Deviations from the energy gap law. *J. Am. Chem. Soc.* **2004**, *126*, 3789−3794.
(26) Yu, X.; Leitner, D. M. Vibrational energy transfer and heat conduction in a protein. *J. Phys. Chem. B* **2003**, *107*, 1698−1707.
(27) Fujisaki, H.; Straub, J. E. Vibrational energy relaxation in proteins. *Proc. Natl. Acad. Sci. U. S. A.* **2005**, *102*, 6726−6731.
(28) Stock, G. Classical simulation of quantum energy flow in biomolecules. *Phys. Rev. Lett.* **2009**, *102*, 118301.
(29) Leitner, D. M. Energy flow in proteins. *Annu. Rev. Phys. Chem.* **2008**, *59*, 233−259.
(30) Radloff, W.; Stert, V.; Freudenberg, Th.; Hertel, I. V.; Jouvet, C.; Dedonder-Lardeux, C.; Solgadi, D. Internal conversion in highly excited benzene and benzene dimer: femtosecond time-resolved photoelectron spectroscopy. *Chem. Phys. Lett.* **1997**, *281*, 20−26.
(31) Mataga, N.; Shibata, Y.; Chosrowjan, H.; Yoshida, N.; Osuka, A. Internal conversion and vibronic relaxation from higher excited electronic state of porphyrins: Femtosecond fluorescence dynamics studies. *J. Phys. Chem. B* **2000**, *104*, 4001−4004.
(32) Lasorne, B.; Sicilia, F.; Bearpark, M. J.; Robb, M. A.; Worth, G. A.; Blancafort, L. Automatic generation of active coordinates for quantum dynamics calculations: Application to the dynamics of benzene photochemistry. *J. Chem. Phys.* **2008**, *128*, 124307.
(33) Soler, M. A.; Roitberg, A. E.; Nelson, T.; Tretiak, S.; Fernandez-Alberti, S. Analysis of State-Specific Vibrations Coupled to the Unidirectional Energy Transfer in Conjugated Dendrimers. *J. Phys. Chem. A* **2012**, *116*, 9802−9810.
(34) Galindo, J.; Fernandez-Alberti, S.; Roitberg, A. Electronic Excited State Specific IR Spectra for Phenylene Ethynylene Dendrimer Building Blocks. *J. Phys. Chem. C* **2013**, *117*, 26517−26528.
(35) Saab, M.; Doriol, L. J.; Lasorne, B.; Guerin, S.; Gatti, F. A quantum dynamics study of the benzopyran ring opening guided by laser pulses. *Chem. Phys.* **2014**, *442*, 93−102.
(36) Lasorne, B.; Worth, G. A.; Robb, M. A. Excited-state dynamics. *WIREs Comput. Mol. Sci.*, **2011**, *1*, 460−475.
(37) Chen, Y.; Palmer, P. M.; Topp, M. R. Infrared Spectroscopy of Jetcooled, Electronically Excited Clusters of Coumarin 151: Excited-state Interactions and Conformational Relaxation. *Int. J. Mass Spectrom.* **2002**, *220*, 231−251.
(38) Weiler, M.; Bartl, K.; Gerhards, M. Infrared/ultraviolet Quadruple Resonance Spectroscopy to Investigate Structures of Electronically Excited States. *J. Chem. Phys.* **2012**, *136*, 114202.
(39) Seurre, N.; Le Barbu-Debus, K.; Lahmani, F.; Zehnacker-Rentien, A.; Sepiol, J. Electronic and Vibrational Spectroscopy of Jet-cooled Mcyanophenol and Its Dimer: Laser-induced Fluorescence and Fluorescence-dip IR Spectra in the S0 and S1 States. *Chem. Phys.* **2003**, *295*, 21−33.
(40) Zhang, Y.; Kubicki, J.; Platz, M. S. Ultrafast UV-Visible and Infrared Spectroscopic Observation of a Singlet Vinylcarbene and the Intramolecular Cyclopropenation Reaction. *J. Am. Chem. Soc.* **2009**, *131*, 13602−13603.
(41) Zhang, Y.; Burdzinski, G.; Kubicki, J.; Vyas, S.; Hadad, C. M.; Sliwa, M.; Poizat, O.; Buntinx, G.; Platz, M. S. Study of the S1 Excited State of para-Methoxy-3-phenyl-3-methyl Diazirine by Ultrafast Time Resolved UV-Vis and IR Spectroscopies and Theory. *J. Am. Chem. Soc.* **2009**, *131*, 13784−13790.
(42) Vyas, S.; Kubicki, J.; Luk, H. L.; Zhang, Y.; Gritsan, N. P.; Hadad, C. M.; Platz, M. S. An Ultrafast Time-resolved Infrared and UV-vis Spectroscopic and Computational Study of the Photochemistry of Acyl Azides. *J. Phys. Org. Chem.* **2012**, *25*, 693−703.
(43) Dougherty, T. P.; Heilweil, E. J. Ultrafast Transient Infrared Absorption Studies of M(CO)6 (M = Cr, Mo or W) Photoproducts in N-hexane Solution. *Chem. Phys. Lett.* **1994**, *227*, 19−25.
(44) Noid, D. W.; Koszykowski, M. L.; Marcus, R. A. Quasiperiodic and Stochastic Behavior in Molecules. *Annu. Rev. Phys. Chem.* **1981**, *32*, 267−309.
(45) Schulz, I. P. A.; Sudbo, S.; Krajnovich, D. J.; Kwok, H. S.; Shen, Y. R.; Lee, Y. T. Multiphoton dissociation of polyatomic molecules. *Annu. Rev. Phys. Chem.* **1979**, *30*, 379−409.
(46) McDonald, J. D. Creation and disposal of vibrational energy in polyatomic molecules. *Annu. Rev. Phys. Chem.* **1979**, *30*, 29−50.
(47) Hill, J. R.; Ziegler, C. J.; Suslick, K. S.; Dlott, D. D.; Rella, C. W.; Fayer, M. D. Tuning the vibrational relaxation of co bound to heme and metalloporphyrin complexes. *J. Phys. Chem.* **1996**, *100*, 18023−18032.
(48) Hamm, P.; Lim, M. H.; Hochstrasser, R. M. Structure of the amide i band of peptides measured by femtosecond nonlinearinfrared spectroscopy. *J. Phys. Chem. B* **1998**, *102*, 6123−6138.
(49) Peterson, K. A.; Rella, C. W.; Engholm, J. R.; Schwettman, H. A. Ultrafast vibrational dynamics of the myoglobin amide i band. *J. Phys. Chem. B* **1999**, *103*, 557−561.
(50) Dlott, D. D. Vibrational energy redistribution in polyatomic liquids: 3d infrared-raman spectroscopy. *Chem. Phys.* **2001**, *266*, 149−166.

DOI: 10.1021/acs.jpcb.5b09548
J. Phys. Chem. B 2016, 120, 49−58

(51) Iwaki, L.; Dlott, D. D. Vibrational energy transfer in condensed phases In *Encyclopedia of chemical physics and physical chemistry*; Moore, J. H., Spencer, N. D., Eds.; IOP Publishing Ltd: Bristol, Vol. 3, pp 2717−2736, 2001.
(52) Fayer, M. D. *Ultrafast infrared and Raman spectroscopy*; Marcel Dekker, Inc.: New York, 2001.
(53) Shigeto, S.; Dlott, D. D. Vibrational relaxation of an amino acid in aqueous solution. *Chem. Phys. Lett.* **2007**, *447*, 134−139.
(54) Wang, Z. H.; Carter, J. A.; Lagutchev, A.; Koh, Y. K.; Seong, N. H.; Cahill, D. G.; Dlott, D. D. Ultrafast flash thermal conductance of molecular chains. *Science* **2007**, *317*, 787−790.
(55) Shigeto, S.; Pang, Y.; Fang, Y.; Dlott, D. D. Vibrational relaxation of normal and deuterated liquid nitromethane. *J. Phys. Chem. B* **2008**, *112*, 232−241.
(56) Fang, Y.; Shigeto, S.; Seong, N.; Dlott, D. D. Vibrational energy dynamics of glycine, n-methylacetamide, and benzoate anion in aqueous (D_2O) solution. *J. Phys. Chem. A* **2009**, *113*, 75−84.
(57) Nguyen, P. H.; Stock, G. Nonequilibrium molecular-dynamics study of the vibrational energy relaxation of peptides in water. *J. Chem. Phys.* **2003**, *119*, 11350−11358.
(58) Brooks, C. L.; Karplus, M.; Pettitt, B. M. Proteins: A Theoretical Perspective of Dynamics, Structure, and Thermodynamics. *Adv. Chem. Phys.* **1988**, *71*, 1−259.
(59) Nishikawa, T.; Gō, N. Normal modes of vibration in bovine pancreatic trypsin inhibitor and its mechanical property. *Proteins: Struct., Funct., Genet.* **1987**, *2*, 308−329.
(60) Brooks, B.; Karplus, M. Harmonic dynamics of proteins: normal modes and fluctuations in bovine pancreatic trypsin inhibitor. *Proc. Natl. Acad. Sci. U. S. A.* **1983**, *80*, 6571−6575.
(61) McCammon, J. A.; Harvey, S. C. *Dynamics of Proteins and Nucleic Acids*; Cambridge University Press: Cambridge, U.K., 1987.
(62) Parameswaran, S.; Wang, R.; Hastings, G. Calculation of the Vibrational Properties of Chlorophyll a in Solution. *J. Phys. Chem. B* **2008**, *112*, 14056−14062.
(63) Nelson, T.; Fernandez-Alberti, S.; Chernyak, V.; Roitberg, A. E.; Tretiak, S. Nonadiabatic excited-state molecular dynamics modeling of photoinduced dynamics in conjugated molecules. *J. Phys. Chem. B* **2011**, *115*, 5402−5414.
(64) Nelson, T.; Fernandez-Alberti, S.; Roitberg, A.; Tretiak, S. Nonadiabatic Excited-State Molecular Dynamics: Modeling Photophysics in Organic Conjugated Materials. *Acc. Chem. Res.* **2014**, *47*, 1155−1164.
(65) Tully, J. C. Molecular-dynamics with electronic-transitions. *J. Chem. Phys.* **1990**, *93*, 1061−1071.
(66) Hammes-Schiffer, S.; Tully, J. C. Proton-transfer in solution - molecular-dynamics with quantum transitions. *J. Chem. Phys.* **1994**, *101*, 4657−4667.
(67) Tretiak, S.; Mukamel, S. Density matrix analysis and simulation of electronic excitations in conjugated and aggregated molecules. *Chem. Rev.* **2002**, *102*, 3171−3212.
(68) Chernyak, V.; Schulz, M. F.; Mukamel, S.; Tretiak, S.; Tsiper, E. V. Krylov-space algorithms for time-dependent hartree-fock and density functional computations. *J. Chem. Phys.* **2000**, *113*, 36−43.
(69) Tretiak, S.; Isborn, C. M.; Niklasson, A. M. N.; Challacombe, M. Representation independent algorithms for molecular response calculations in time-dependent self-consistent field theories. *J. Chem. Phys.* **2009**, *130*, 054111.
(70) Furche, F.; Ahlrichs, R. Adiabatic time-dependent density functional methods for excited state properties. *J. Chem. Phys.* **2002**, *117*, 7433−7447.
(71) Tretiak, S.; Chernyak, V. Resonant nonlinear polarizabilities in the time-dependent density functional theory. *J. Chem. Phys.* **2003**, *119*, 8809−8823.
(72) Tommasini, M.; Chernyak, V.; Mukamel, S. Electronic density-matrix algorithm for nonadiabatic couplings in molecular dynamics simulations. *Int. J. Quantum Chem.* **2001**, *85*, 225−238.
(73) Chernyak, V.; Mukamel, S. Density-matrix representation of nonadiabatic couplings in time-dependent density functional (TDDFT) theories. *J. Chem. Phys.* **2000**, *112*, 3572−3579.
(74) Send, R.; Furche, F. First-order nonadiabatic couplings from time-dependent hybrid density functional response theory: Consistent formalism, implementation, and performance. *J. Chem. Phys.* **2010**, *132*, 044107.
(75) Mukamel, S. Photochemistry - trees to trap photons. *Nature* **1997**, *388*, 425−427.
(76) Mukamel, S.; Tretiak, S.; Wagersreiter, T.; Chernyak, V. Electronic coherence and collective optical excitations of conjugated molecules. *Science* **1997**, *277*, 781−787.
(77) Tretiak, S.; Chernyak, V.; Mukamel, S. Recursive density-matrix-spectral-moment algorithm for molecular nonlinear polarizabilities. *J. Chem. Phys.* **1996**, *105*, 8914−8928.
(78) Tretiak, S.; Zhang, W. M.; Chernyak, V.; Mukamel, S. Excitonic couplings and electronic coherence in bridged naphthalene dimers. *Proc. Natl. Acad. Sci. U. S. A.* **1999**, *96*, 13003−13008.
(79) Dewar, M. J. S.; Zoebisch, E. G.; Healy, E. F.; Stewart, J. J. P. AM1: A new general purpose quantum mechanical model. *J. Am. Chem. Soc.* **1985**, *107*, 3902−3909.
(80) Stewart, J. J. P. Optimization of parameters for semiempirical methods IV: extension of MNDO, AM1, and PM3 to more main group elements. *J. Mol. Model.* **2004**, *10*, 155−164.
(81) Shavitt, I. *Modern Theoretical Chemistry*; Plenum Press: New York, 1976.
(82) Szalay, P. G.; Müller, T.; Gidofalvi, G.; Lischka, H.; Shepard, R. Multiconfiguration self-consistent field and multireference configuration interaction methods and applications. *Chem. Rev.* **2012**, *112*, 108−181.
(83) Reynolds, C. H. An AM1 theoretical study of the structure and electronic properties of porphyrin. *J. Org. Chem.* **1988**, *53*, 6061−6064.
(84) Zandler, M. E.; D'Souza, F. Electronic and structural properties of the metalloporphyrin structural isomers: Semiempirical AM1 and PM3 calculations. *J. Mol. Struct.: THEOCHEM* **1997**, *401*, 301−314.
(85) Katagi, T. Semi-empirical am1 and pm3 calculations of five- and six-coordinate oxo iron (iv) porphyrin complexes. *J. Mol. Struct.: THEOCHEM* **2005**, *728*, 49−56.
(86) Stewart, J. J. P. Optimization of parameters for semiempirical methods I. method. *J. Comput. Chem.* **1989**, *10*, 209−220.
(87) Stewart, J. J. P. Optimization of parameters for semiempirical methods II. applications. *J. Comput. Chem.* **1989**, *10*, 221−264.
(88) Stewart, J. J. P. Optimization of parameters for semiempirical methods III. extension of PM3 to Be, Mg, Zn, Ga, Ge, As, Se, Cd, In, Sn, Sb, Te, Hg, Tl, Pb, and Bi. *J. Comput. Chem.* **1991**, *12*, 320−341.
(89) Linnanto, J.; Korppi-Tommola, J. Spectroscopic properties of Mg-chlorin, Mg-porphyrin and chlorophylls *a*, *b*, *c*1, *c*2, *c*3 and *d* studied by semi-empirical and *ab initio* MO/CI methods. *Phys. Chem. Chem. Phys.* **2000**, *2*, 4962−4970.
(90) Linnanto, J.; Korppi-Tommola, J. Spectroscopic properties of mg-chlorin, mg-bacterochlorin and bacteriochlorophylls *a*, *b*, *c*, *d*, *e*, *f*, *g*, and *h* studied by semiempirical and *ab initio* MO/CI methods. *J. Phys. Chem. A* **2001**, *105*, 3855−3866.
(91) Linnanto, J.; Korppi-Tommola, J. Quantum chemical simulation of excited states of chlorophylls, bacteriochlorophylls and their complexes. *Phys. Chem. Chem. Phys.* **2006**, *8*, 663−687.
(92) Hutter, M. C.; Reimers, J. R.; Hush, N. S. Modeling the bacterial photosynthetic reaction center. 1. magnesium parameters for semi-empirical AM1 method developed using a genetic algorithm. *J. Phys. Chem. B* **1998**, *102*, 8080−8090.
(93) Verlet, L. Computer "experiments" on classical fluids. I. thermodynamical properties of Lennard-Jones molecules. *Phys. Rev.* **1967**, *159*, 98−103.
(94) Allen, M. P.; Tildesley, D. J. *Computer Simulation of Liquids*; Clarendon Press: Oxford, U.K., 1987.
(95) Paterlini, M. G.; Ferguson, D. M. Constant temperature simulations using the Langevin equation with velocity Verlet integration. *Chem. Phys.* **1998**, *236*, 243−252.
(96) Hull, E.; Enright, W. H.; Jackson, K. R. *User's guide for DVERK - A subroutine for solving non-stiff ODEs*; Technical Report 100; Department of Computer Science, University of Toronto: Toronto, Canada, 1976.

DOI: 10.1021/acs.jpcb.5b09548
J. Phys. Chem. B 2016, 120, 49−58

(97) Nelson, T.; Fernandez-Alberti, S.; Chernyak, V.; Roitberg, A. E.; Tretiak, S. Nonadiabatic excited-state molecular dynamics: Numerical tests of convergence and parameters. *J. Chem. Phys.* **2012**, *136*, 054108.
(98) Wu, C.; Malinin, S. V.; Tretiak, S.; Chernyak, V. Y. Multiscale Modeling of Electronic Excitations in Branched Conjugated Molecules Using an Exciton Scattering Approach. *Phys. Rev. Lett.* **2008**, *100*, 057405.
(99) Ditchfield, R.; Hehre, W. J.; Pople, J. A. Self-consistent molecular-orbital methods. IX. An extended Gaussian-type basis for molecular-orbital studies of organic molecules. *J. Chem. Phys.* **1971**, *54*, 724−728.
(100) Hehre, W. J.; Ditchfield, R.; Pople, J. A. Self-consistent molecular orbital methods. XII. Further extensions of Gaussian-type basis sets for use in molecular orbital studies of organic molecules. *J. Chem. Phys.* **1972**, *56*, 2257−2261.
(101) Hariharan, P. C.; Pople, J. A. The influence of polarization functions on molecular orbital hydrogenation energies. *Theor. Chem. Acc.* **1973**, *28*, 213−222.
(102) Becke, A. D. Density-functional thermochemistry. III. the role of exact exchange. *J. Chem. Phys.* **1993**, *98*, 5648−5652.
(103) Frisch, M. J.; Trucks, G. W.; Schlegel, H. B.; Scuseria, G. E.; Robb, M. A.; Cheeseman, J. R.; Scalmani, G.; Barone, V.; Mennucci, B.; Petersson, G. A., et al. *Gaussian 09*, Revision A.02; Gaussian, Inc.: Wallingford, CT, 2009.
(104) Fernandez-Alberti, S.; Roitberg, A. E.; Nelson, T.; Tretiak, S. Shishiodoshi unidirectional energy transfer mechanism in phenylene ethynylene dendrimers. *J. Chem. Phys.* **2012**, *137*, 014512.
(105) Tully, J. C. Nonadiabatic molecular dynamics. *Int. J. Quantum Chem.* **1991**, *40* (S25), 299−309.
(106) Hack, M. D.; Jasper, A. W.; Volobuev, Y. L.; Schwenke, D. W.; Truhlar, D. G. Quantum Mechanical and Quasiclassical Trajectory Surface Hopping Studies of the Electronically Nonadiabatic Predissociation of the Ã State of NaH_2. *J. Phys. Chem. A* **1999**, *103*, 6309−6326.

DOI: 10.1021/acs.jpcb.5b09548
J. Phys. Chem. B 2016, 120, 49−58